



Friction and wear characteristics of aluminum bronze (QA110-4-4) bearing materials under high-temperature dry sliding conditions

Hui Li^{1,2} · Ruiqin Li¹ · Feng Yang³ · Dongguang Zhang⁴ · Jianwei Zhang¹

Received: 23 December 2019 / Accepted: 25 May 2020 / Published online: 8 June 2020
© The Brazilian Society of Mechanical Sciences and Engineering 2020

Abstract

The friction and wear characteristics of aluminum bronze QA110-4-4 bearing materials are investigated through pin–disk simulation testing under the dry sliding state at the operating conditions with rotating speed, load and temperature using the high-speed and high-temperature friction and wear testing machine (MG-2000). The quality of the pin, the friction coefficient and surface topography of the samples are monitored during the tests. The study results show that the average friction coefficient presents a similar N shape curve with the increase in rotating speed and temperature and a hook shape curve with the increase in load. The wear extent increases linearly with the increase in rotating speed, increases firstly and then decreases with the increase in load and presents a similar N shape trend with the increase in temperature. The main wear mechanisms of QA110-4-4 bearing materials under high-temperature dry sliding conditions are discussed; the rotating speed mainly influences the friction and wear characteristics of the material by sliding heat. The loads mainly affect the friction and wear characteristics of the material through the actual contact area, and wear debris. The influence of temperature on the friction and wear characteristics of the material mainly depended on the surface layer properties.

Keywords Aluminum bronze (QA110-4-4) · Dry sliding · Friction coefficient · Wear extent

1 Introduction

Aluminum bronze QA110-4-4 has many advantages such as high strength, good friction reduction, high-temperature mechanical properties and corrosion resistance [1–5], which is widely used to fabricate high-strength wear-resistant parts and engineering devices under high-temperature conditions. However, the low tribological properties of aluminum bronze hinder the further application of aluminum bronze.

Among the joint bearing of the robots, aluminum bronze is the most commonly used bearing material. The bearing performance is closely related to the friction and wear performance of the used aluminum bronze [6, 7]. Hence, to gain better friction–wear properties of aluminum bronze, changing microstructure of the material is an effective method. Li et al. [8, 9] analyzed the effects of grain refinement and microstructure on mechanical and tribological behaviors of aluminum bronze modified by Ti and B. The friction coefficients, wear extent and mechanical characteristics are strongly dependent on the volume fraction of α -phase present in the alloy and less dependent on the average α -phase size. Li also developed a high-strength wear-resistant aluminum bronze, which has better friction and wear properties than other aluminum bronze materials of the same class. Prasad [10] investigated sliding wear behaviors of bronzes with different material test conditions, composition, and microstructure. They reported that there is no direct correlativity between the mechanical properties (such as elongation, tensile strength and hardness) and wear response of the test specimens. In addition, no matter the material microstructure and composition, there is a particular set of test conditions, resulting in the best wear performance. Türk et al. [11]

Technical Editor: Izabel Fernanda Machado, Dr.

✉ Ruiqin Li
liruiqin@nuc.edu.cn

¹ School of Mechanical Engineering, North University of China, Taiyuan 030051, China

² Department of Mining Engineering, Lvliang University, Lvliang 033001, China

³ Shanghai Xinli Power Equipment Research Institute, Shanghai 200125, China

⁴ College of Mechanical and Vehicle Engineering, Taiyuan University of Technology, Taiyuan 030024, China

studied the effects of tin, cadmium and lead on the microstructure of improved ZA-8 alloy. The tribological properties of traditional bearing bronze were measured under the same conditions to verify the effect of trace elements on the tribological properties of improved ZA-8 alloy. The ZA-8 alloy and improved with Sn, Cd and Pb alloys showed higher wear resistance when compared with bearing bronze. Alemdağ et al. [12] prepared one binary Al-40Zn alloy with different mass percentages of copper and five ternary Al-40Zn-Cu alloys with different mass percentages of copper through using permanent mold casting.

The friction and wear characteristics of the ternary alloy were studied by using a coordinated block disk tester machine and compared with the results of SAE 65 bearing bronze. The results showed that the highest mechanical strength and wear-resisting properties were picked up with the Al-40Zn-3Cu alloy. Recent research has found that the addition of different coating materials to the metal surface can increase the wear-resisting properties of the material. Alam et al. [13] researched friction–wear properties of aluminum bronze coatings upon steel substrates sprayed through a low-pressure plasma technique. It was observed that this material has many advantages, such as dense microstructure, high hardness, low coefficient of friction and good wearing resistance, under the optimum operating conditions. Guo et al. [14] investigated the microscopic constructions and friction behavior of tin–bronze-based composite coatings by cold spray. The results showed that the friction coefficient and wear rate of bronze composite coating are lower than the bronze/TiN coating. Miguel et al. [15] reported the friction behavior of bronze composite coatings obtained to employ plasma thermal spraying techniques. It is found that the addition of alumina in bronze coatings significantly improved its wear resistance.

The above researches tried to improve the friction–wear properties of aluminum bronze, mainly by changing the performance of the friction surface. Because friction and wear are not the inherent characteristics of the material but depend on the sliding conditions and the counterpart material, it is particularly important to study the influence of working conditions on the friction–wear properties of aluminum bronze [16–20]. However, there is a lack of published work concerning dry sliding friction–wear behaviors of aluminum bronze sliding bearing alloy at elevated temperatures.

In this study, with pins made of QAl10-4-4, the pin-on-disk sliding tests are implemented under different rotating speed, loading and temperature conditions, where we

analyze the evolution of the friction coefficient with time, as well as the evolution of pin mass after the end of the test. These tests are aimed to investigate the effect of working conditions on dry sliding friction and wear behaviors of aluminum bronze sliding bearing alloy while providing a theoretical basis for practical application of aluminum bronze bearing alloy.

2 Design of experiments

2.1 Aluminum bronze QAl10-4-4

Aluminum bronze QAl10-4-4 in the extruded state is rapidly cooled in the water at 10–35 °C after solid solution at 900 °C for 2 h. Then, aging treatment is performed at 450 °C for 1 h, and the sample pin is taken out and air-cooled to room temperature. After machining the sample pin, its hardness is measured at 220 HB. The chemical composition of QAl10-4-4 is depicted in Table 1.

2.2 Test conditions

Dry friction pin–disk simulation tests are conducted on a high-speed and high-temperature friction and wear testing machine MG-2000 (Fig. 1) to examine the friction and wear characteristics of QAl10-4-4 at high temperatures. The rotating speed, pressure and temperature of the setting are in ranges of 0–6000 rpm, 0–2000 N and 0–800 °C, respectively. The pin diameter, friction disk thickness and rotating radius are 10, 10 and 30 mm, respectively. The friction disk is composed of 40Cr after quenching at 850 °C and low temperature at 150 °C. 40Cr is a kind of alloy structural steel with nice mechanical properties after tempering treatment. The chemical composition of 40Cr is depicted in Table 2.

All test samples are made from the same batch of heat-treated materials. The end surface of the sample pin is polished to ensure that the roughness values of the end surfaces of the sample pin and sample disk are less than 0.08 and 0.02 μm , respectively. The surface topography of the sample pin is characterized using a high-power optical microscope, as shown in Fig. 2.

2.3 Test scheme

The single-factor design method is used to investigate the influences of operating conditions (rotation speed ω , load f

Table 1 Chemical composition of aluminum bronze QAl10-4-4

Element	Cu	Sn	Zn	Pb	P	Ni	Al	Fe	Mn	Si	Sum of impurities
Weight fraction/%	allowance	0.1	0.5	0.02	0.01	3.5~5.5	9.5~11.0	3.5~5.5	0.3	0.1	1.0

Fig. 1 High-speed and high-temperature friction and wear testing machine (MG-2000)

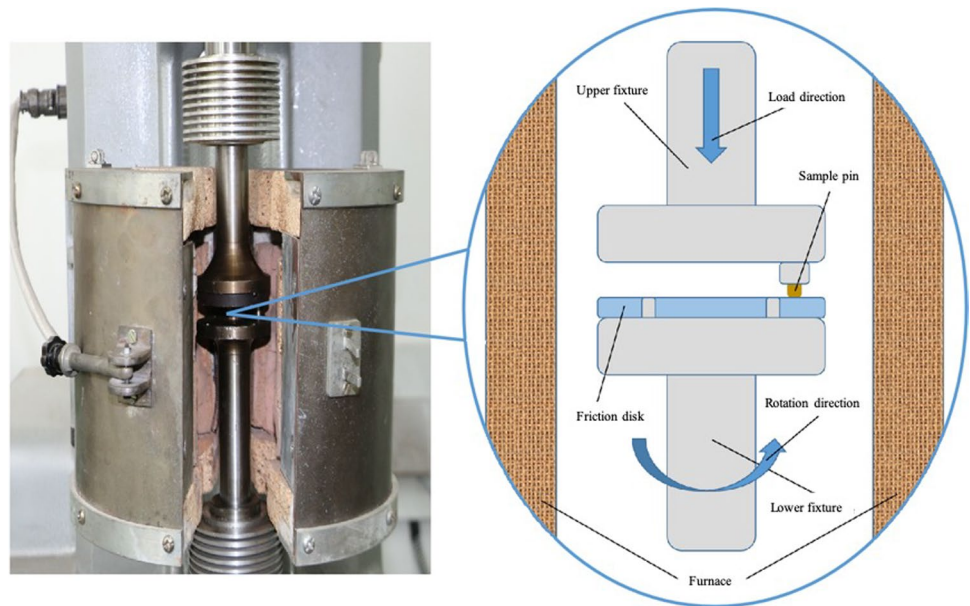


Table 2 Chemical composition of 40Cr

Element	Fe	C	Si	Mn	Cr	Ni	P	S	Cu	Mo
Weight fraction/%	allowance	0.37~0.44	0.17~0.37	0.50~0.80	0.80~1.10	≤0.30	≤0.035	≤0.035	≤0.030	≤0.10

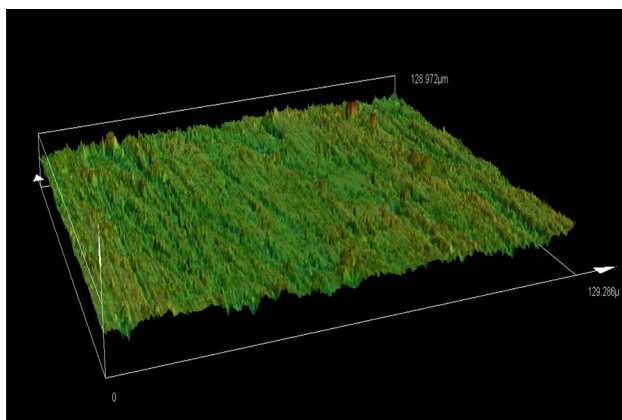


Fig. 2 The surface topography of the sample pin

and temperature T) on the friction coefficient μ (or average friction coefficient $\bar{\mu}$) and the wear extent Δm of the sample pin. Table 3 shows the test schemes.

The test procedures are as follows:

1. The surface of the new sample pin and disk is cleaned by alcohol. The weight of the sample pin is recorded as m_q after drying.
2. The sample pin and disk are installed. The loading force, ambient temperature, rotation speed and running time are set.
3. The testing machine starts after the temperature is stable. The temperature, friction moment and friction coefficient of the sample pin are recorded.
4. The friction pair is separated after the test, the sample pin is cleaned and dried after cooling, and the new weight of the pin is recorded after the test as m_h . Then, the wear extent can be calculated by $\Delta m = m_q - m_h$.

Table 3 Parameters of single-factor test

Test No.	Rotation speed ω /rpm	Load f /N	Temperature T /°C
1	150, 200, 250, 300, 350	120	200
2	250	40, 80, 120, 160, 200	200
3	250	120	100, 150, 200, 250, 300

3 Results and analysis

3.1 Friction coefficient analysis

The test results in Fig. 3 show that the friction coefficient curve increases sharply at the beginning. The main reason is that a large number of rough peaks exist on the contact surface, the actual contact area is remarkably smaller than the apparent contact area, and many phenomena occur on the two contact surfaces, such as mutual extrusion and mutual embedding. In the following friction process, the rough peaks of the contact surface are smoothed, and its smoothness is improved, resulting in a decrease in the friction coefficient [21, 22]. Moreover, friction will generate substantial sliding heat, leading to increased temperature of the contact surface, softening, and reduced shear strength of the rough peak, thereby decreasing the friction coefficient. In the end, the friction coefficient curve rapidly declines with the increase in friction time and gradually fluctuates up and down the fixed value because the entire

process is composed of different friction forms. As the friction process continues, the proportion of various friction forms will change, and alternations and interactions occur among them, thereby fluctuating the friction coefficient. Furthermore, given that the oxide film on the metal contact surface is an alternating cycle of formation and failure in the entire friction process, the existence of the oxide film will reduce the friction coefficient and is the primary reason for its fluctuation [23–25].

Figure 4 shows the average friction coefficient under stable friction and wear stage (300–600 s of the results in Fig. 3). In Fig. 4a, when the rotating speed is low at the beginning ($\omega = 150$ rpm), friction mainly occurs between the surface oxide films which plays a role in reducing friction and resistance. Hence, the average friction coefficient is small ($\bar{\mu} = 0.0544$) at this time. Before the rotation speed increases to $\omega = 200$ rpm, the increase in wear debris makes the metal matrix on the contact surface exposed, and the contact surface becomes rough, thereby increasing the average friction coefficient. After that, when the rotating speed increases further, the increase in sliding heat release makes

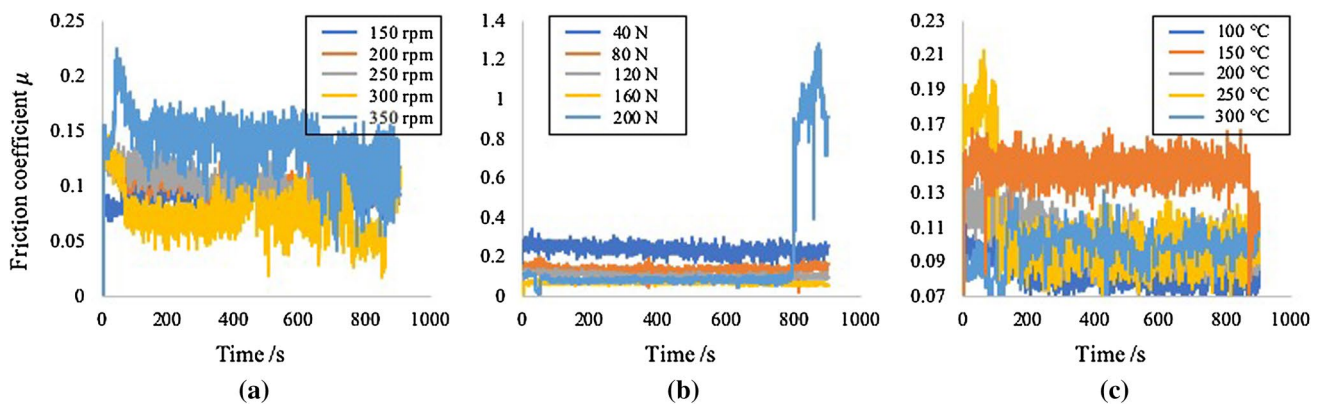


Fig. 3 Influence of different operating conditions on friction coefficient: **a** speeds, **b** loads and **c** temperatures

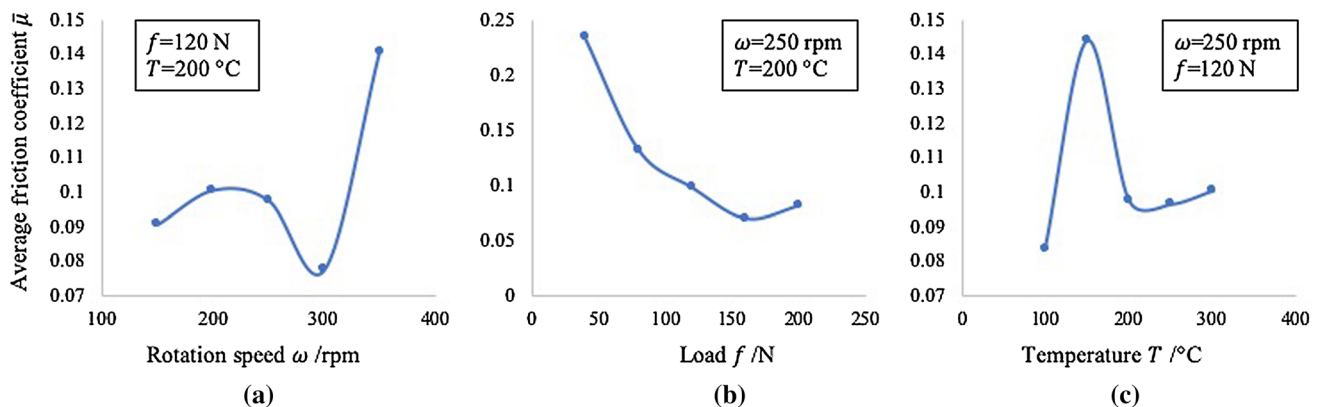


Fig. 4 Variation of average friction coefficient $\bar{\mu}$ under different operating conditions: **a** rotation speeds, **b** loads and **c** temperatures

the contact surface temperature increase. Consequently, the metal matrix becomes prone to oxidation and the oxide film is produced. Therefore, the average friction coefficient presents a decreasing trend and the average friction coefficient reaches a minimum ($\bar{\mu}=0.0744$) at $\omega=300$ rpm. However, when the rotating speed is excessively high, the intensification of metal softening leads to adhesive wear between the contact surfaces and a sharp increase in the average friction coefficient. When the rotating speed ω increases after 300 rpm, the average friction coefficient increases sharply to $\bar{\mu}=0.1421$ at $\omega=350$ rpm. In Fig. 4b, when the load is low, the low pressure on the contact surfaces makes the compressive stress of each rough peak small and the depth of mutual embedding shallow. Hence, the actual contact area is small. Besides, under the action of minimal compressive stress, the large shear force on the rough peak makes the average friction coefficient large. With the increase in load, the number and size of contact points increase, thereby increasing the actual contact area. Moreover, the oxide wear debris produced by friction reduces the friction and resistance between the contact surfaces. Thus, when the load increases to $f=160$ N, the average friction coefficient reaches a minimum ($\bar{\mu}=0.0696$). The average friction coefficient increases slightly when the load f is more than 160 N and reaches $\bar{\mu}=0.0736$ at $f=200$ N. The excessive load causes the compressive stress of the contact surface to exceed its hardness value. Besides, the serious plastic deformation of the material is serious results in a slight bonding effect. Thus, the average friction coefficient increases. In Fig. 4c, the influence of temperature on the friction coefficient of materials is closely related to the change of the contact surface. At $T=100$ °C, friction mainly occurs between the oxide layers on the surface, the average friction coefficient is low ($\bar{\mu}=0.0851$). As the temperature T increases to 150 °C, the average friction coefficient $\bar{\mu}$ increases sharply to 0.1423. When the temperature T increases to 200 °C, the elastic-plastic deformation of the metal changes, the decrease

in elastic and the increase in plasticity makes the friction scope expand, where the friction also exists between the oxide film and metal and between metal and metal, leading to an increase in the average friction coefficient. With the further increase in temperature, the exposed metal becomes prone to oxidation reaction, thereby forming oxides, which leads to a decrease in the average friction coefficient and reaches a minimum $\bar{\mu}=0.0964$ at $T=250$ °C. Over 250 °C, metal softening and adhesive wear intensify, thereby increasing the average friction coefficient.

3.2 Wear analysis

Figure 5 shows the change of the wear extent with the operating conditions. In Fig. 5a, the measurement results show that the wear extent generally increases linearly with the increase in rotating speed. On the basis of Archard's wear law, the wear extent is proportional to the sliding distance [26]. The increase in the rotating speed increases the temperature on the contact surface, which results in the oxidation of the material and spalling of the oxide layer. Hence, the adhesive wear proportional to the temperature. In Fig. 5b, when the load is relatively small, the wear is mainly the contact of surface oxide, where the wear debris is mainly a single oxide, the wear extent is small ($\Delta m=0.1555$ g at $f=40$ N). When the load exceeds a certain critical value ($f=80$ N), the wear debris increases. At this moment, the wear extent increases to $\Delta m=0.14888$ g and the wear is based on the metal matrix. In the high-temperature environment produced by sliding heat, the wear debris is mainly a mixture of Al, Cu, Fe, Mn and other metals and its various oxides, which lubricates the contact surfaces and leads to the decrease in wear extent. With the continuous increase in load, the proportion of this mixture increases. Hence, the wear extent decreases with the increase in load. In Fig. 5c, when the temperature T is in the range of 100–200 °C, the contact of rough surface peak intensity is relatively high,

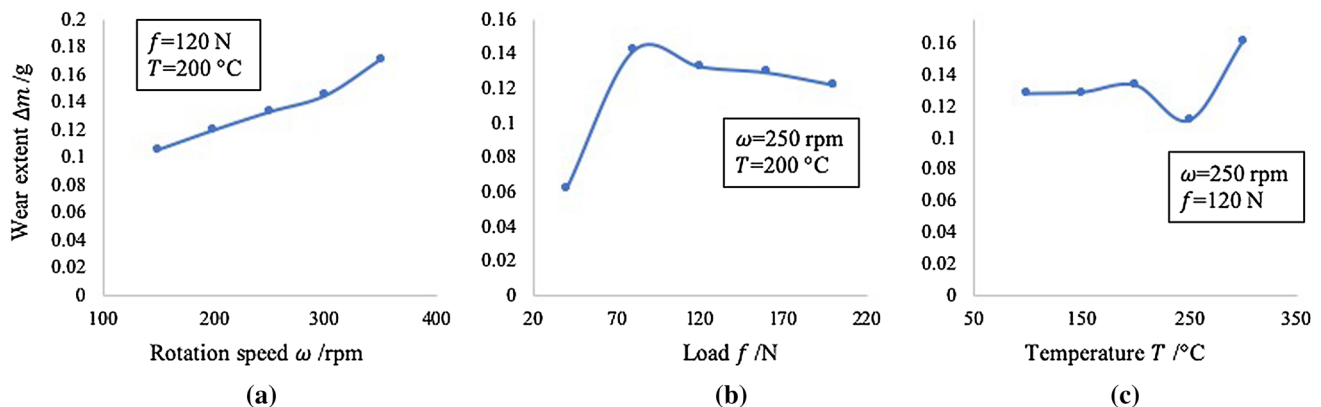


Fig. 5 Variation of wear extent under different operating conditions: **a** rotating speeds, **b** loads and **c** temperatures

making the actual contact area decrease and strengthening the shear resistance of rough peaks. Hence, the wear form is mainly the micro-cutting caused by abrasive wear. Besides, with the increase in the temperature, the bare metal matrix becomes prone to oxidation, thereby causing oxidation wear and increasing the wear extent. When the temperature increases further ($T = 250\text{ }^{\circ}\text{C}$), the metal material softens the strength of rough peak decreases, making the actual contact area increase and the abrasive wear decrease. At this time, the wear form is mainly oxidation wear, reducing the wear extent. When the temperature is excessively high ($T = 300\text{ }^{\circ}\text{C}$), the softening of metal materials intensifies. At this time, the wear form is mainly adhesive wear, increasing the wear extent.

3.3 SEM analysis of wear surfaces

The friction sample pin surface was observed under a JSM-7100F scanning electron microscope. Figure 6 presents the SEM images of the sample pin surface at different rotating speeds. At $\omega = 150\text{ rpm}$, the wear on the sample pin surface is mainly oxidation wear. At $\omega = 250\text{ rpm}$, the sample pin surface shows an evident scale-layer distribution along the sliding direction. When the rotating speed ω increases to 350 rpm , the scale-layer distribution of the sample pin surface along the sliding direction becomes wider. The scale edge of the sample pin surface is smoother than that at

$\omega = 250\text{ rpm}$. The reason is that the sliding heat is proportional to the rotating speed, resulting in high temperature on the sample pin surface. Figure 7 shows the SEM images of the sample pin surface at different loads. At $f = 40\text{ N}$, the sample pin surface is smooth and even with additional areas of oxidation wear. At $f = 120\text{ N}$, the sample pin surface has an evident squamous-layer distribution along the sliding direction. At $f = 200\text{ N}$, the scaly-stratiform distribution on the sample pin surface along the sliding direction enlarges and deepens. Figure 8 depicts the SEM images of the sample pin surface at different temperatures. With the increase in temperature, the scaly-stratiform distribution of the sample pin surface enlarges, deepens, and widens along the sliding direction.

3.4 EDS analysis of wear surfaces

The energy spectrum analysis of the sample pin surface after friction was performed using a JSM-7100F scanning electron microscope. Table 4 shows the EDS results of the sample pin surface at different rotating speeds. When the $\omega = 350\text{ rpm}$, the exposed metal matrix is further prone to oxidation because of the increase in sliding heat at high speed, thereby enriching the Oxygen on the sample pin surface. Thus, the wear form is mainly adhesive wear. Table 5 shows the EDS results of the sample pin surface at different loads. When the load is 200 N , the

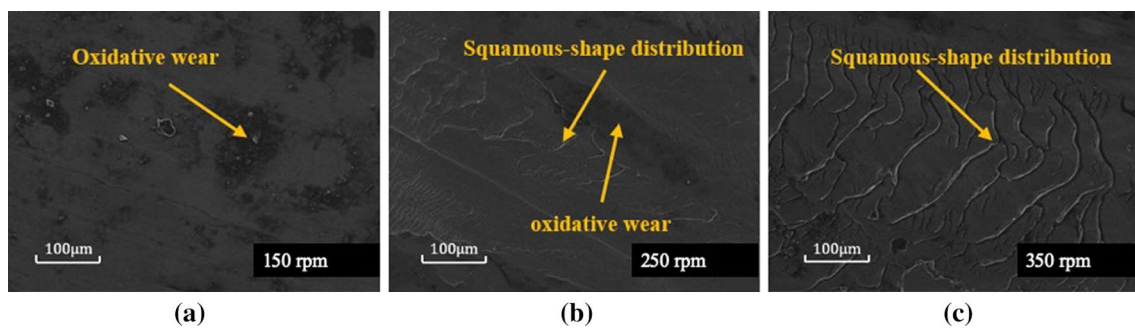


Fig. 6 SEM images at different rotation speeds ω : **a** 150 rpm, **b** 250 rpm and **c** 350 rpm

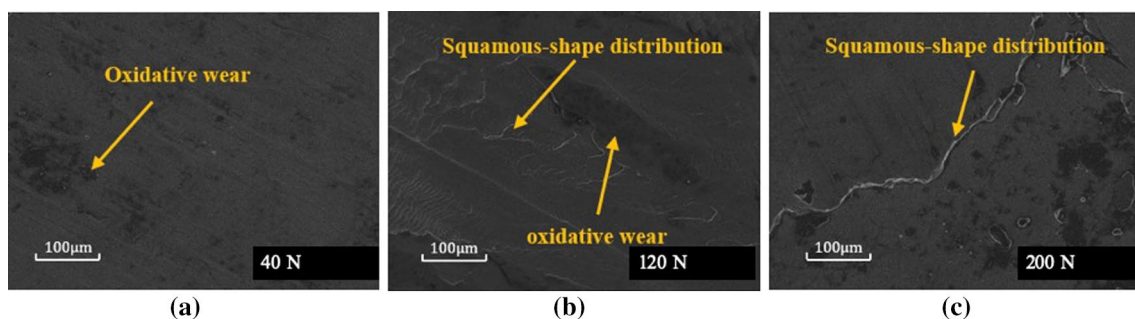


Fig. 7 SEM images at different loads f : **a** 40 N, **b** 120 N and **c** 200 N

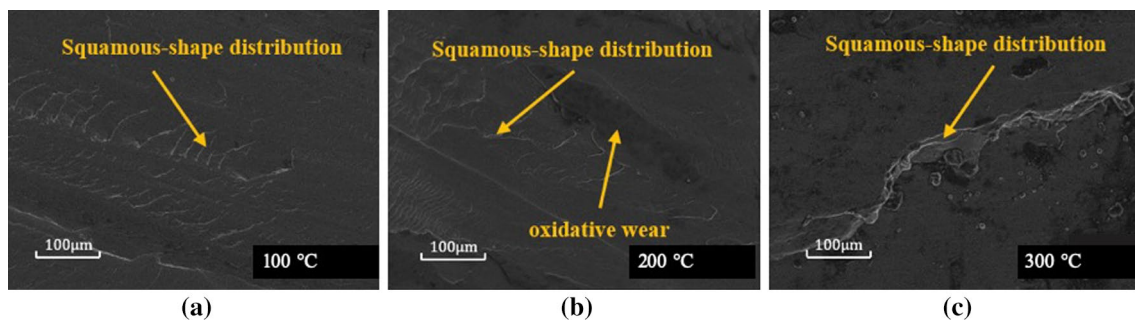


Fig. 8 SEM images at different temperatures T : **a** 100 °C, **b** 200 °C and **c** 300 °C

Table 4 EDS results at different rotation speeds ω

Rotation speed ω /rpm	Cu/%	O/%	Al/%	Fe/%
150	65.03	19.28	11.11	4.58
250	56.86	23.75	9.36	10.03
350	58.23	29.00	9.52	3.25

Table 5 EDS results at different loads f

Loads f /N	Cu/%	O/%	Al/%	Fe/%
40	65.04	17.89	10.73	6.34
120	56.86	23.75	9.36	10.03
200	51.62	37.63	9.14	1.61

Table 6 EDS results at different temperatures T

Temperatures T /°C	Cu/%	O/%	Al/%	Fe/%
100	64.34	24.03	9.69	1.94
200	56.86	23.75	9.36	10.03
300	57.83	26.87	8.84	6.46

high compressive stress on the contact surface enlarges the plastic shape variable of the rough peak of the contact surface, increasing the exposed amount of metal matrix and the amount of wear debris as well as its types, the plastic deformation leads to a large amount of heat generated on the contact surface, resulting in the enrichment of oxygen on the sample pin surface. Table 6 shows the EDS images of the sample pin surface at different temperatures. When the temperature is low, the wear form is mainly abrasive wear as the material is hard. With the increase in temperature, the metal material is softened, decreasing the abrasive wear and increasing the proportion of adhesive wear. The increase in the susceptibility of the exposed metal matrix to react with oxygen at high temperatures forms

an oxide film with lubrication property and increasing the content of Oxygen.

4 Conclusions

A pin–disk test of the aluminum bronze QA110-4-4 commonly used in joint bearings of rescue robots was conducted on a high-speed and high-temperature friction and wear testing machine (MG-2000). This test aims to explore the influences of rotating speed, load and temperature on the high-temperature dry sliding friction and wear characteristics of the material. The main conclusions are as follows: (1) The average friction coefficient first increases, then decreases and then increases again with the increase in rotating speed; and it reaches the minimum value when the rotating speed is 300 rpm. The average friction coefficient first decreases and then increases with the increase in load, and it reaches the minimum value when the load is 160 N. The average friction coefficient first increases, then decreases and then increases with the increase in temperature, and it reaches the minimum value when the temperature is 100 °C. (2) The wear extent increases linearly with the increase in rotating speed. This phenomenon conforms to Archard's wear law. With the increase in load, the wear extent first increases and then decreases, mainly due to the change in the property of wear debris. The wear extent first increases, then decreases and then increases with the increase in temperature, mainly because the temperature changes the elastic–plastic deformation of the contact surface of the material, which leads to the constant change in the wear form. (3) Rotating speed mainly affects the friction and wear characteristics of the material through sliding heat. With the increase in rotating speed, the wear form of the material is transformed into oxidative wear → adhesive wear → oxidative wear → adhesive wear. The load mainly affects the friction and wear characteristics of the material through the actual contact area and debris properties. With the increase in load, the wear form of the material is transformed into oxidative wear → adhesive wear. Temperature mainly affects the friction and wear

characteristics of the material through the surface layer properties. With the increase in temperature, the wear form of the material is transformed into oxidative wear → abrasive wear → adhesive wear.

Acknowledgements The work was financially supported by Scientific and Technological Innovation Programs of Higher Education Institutions in Shanxi (No. 2019L0978) and the Key Research and Development Program of Shanxi Province of China (International Cooperation, 201803D421028, 201903D421051).

References

1. Taga Y, Isogai A, Nakajima K (1977) The role of alloying elements in the friction and wear of copper alloys. *Wear* 44(2):377–391. [https://doi.org/10.1016/0043-1648\(77\)90152-1](https://doi.org/10.1016/0043-1648(77)90152-1)
2. Vander Heide E, Stam ED, Giraud H, Lovato et al (2006) Wear of aluminium bronze in sliding contact with lubricated stainless steel sheet material. *Wear* 261(1):68–73. <https://doi.org/10.1016/j.wear.2005.09.023>
3. Thapliyal S, Dwivedi DK (2017) On cavitation erosion behavior of friction stir processed surface of cast nickel aluminium bronze. *Wear* 376:1030–1042. <https://doi.org/10.1016/j.wear.2017.01.030>
4. Gronostajski J, Chmura W, Gronostajski Z (2002) Bearing materials obtained by recycling of aluminium and aluminium bronze chips. *J Mater Proc Technol* 125:483–490. [https://doi.org/10.1016/S0924-0136\(02\)00326-6](https://doi.org/10.1016/S0924-0136(02)00326-6)
5. Chmura W, Gronostajski Z (2006) Bearing composites made from aluminium and aluminium bronze chips. *J Mater Proc Technol* 178(1–3):188–193. <https://doi.org/10.1016/j.jmatprotec.2006.03.156>
6. Kimura T, Shimizu K, Terada K (2007) Sliding wear characteristic evaluation of copper alloy for bearing. *Wear* 263(1–6):586–591. <https://doi.org/10.1016/j.wear.2007.02.012>
7. Quinlan, John R (1976) Aluminum bronze bearing. U.S. Patent No. 3,995,917.
8. Li Y, Ngai TL (1996) Grain refinement and microstructural effects on mechanical and tribological behaviours of Ti and B modified aluminium bronze. *J Mater Sci* 31(20):5333–5338. <https://doi.org/10.1007/BF01159301>
9. Li Y, Ngai TL, Xia W (1996) Mechanical, friction and wear behaviors of a novel high-strength wear-resisting aluminum bronze. *Wear* 197(1–2):130–136. [https://doi.org/10.1016/0043-1648\(95\)06890-2](https://doi.org/10.1016/0043-1648(95)06890-2)
10. Prasad BK (2004) Sliding wear behaviour of bronzes under varying material composition, microstructure and test conditions. *Wear* 257(1–2):110–123. <https://doi.org/10.1016/j.wear.2003.10.021>
11. Türk A, Kurnaz C, Şevik H (2007) Comparison of the wear properties of modified ZA-8 alloys and conventional bearing bronze. *Mater Des* 28(6):1889–1897. <https://doi.org/10.1016/j.matdes.2006.04.010>
12. Alemdağ Y, Savaşkan T (2009) Mechanical and tribological properties of Al–40Zn–Cu alloys. *Tribol Int* 42(1):176–182. <https://doi.org/10.1016/j.triboint.2008.04.008>
13. Alam S, Sasaki S, Shimura H (2001) Friction and wear characteristics of aluminum bronze coatings on steel substrates sprayed by a low pressure plasma technique. *Wear* 248(1–2):75–81. [https://doi.org/10.1016/S0043-1648\(00\)00520-2](https://doi.org/10.1016/S0043-1648(00)00520-2)
14. Guo X, Zhang G, Li W et al (2009) Investigation of the microstructure and tribological behavior of cold-sprayed tin-bronze-based composite coatings. *App Surf Sci* 255(6):3822–3828. <https://doi.org/10.1016/j.apsusc.2008.10.041>
15. Miguel JM, Vizcaino S, Lorenzana C et al (2011) Tribological behavior of bronze composite coatings obtained by plasma thermal spraying. *Tribol Lett* 42(3):263–273. <https://doi.org/10.1007/s11249-011-9769-7>
16. Rahaman ML, Zhang LC, Ruan HH (2013) Understanding the friction and wear mechanisms of bulk metallic glass under contact sliding. *Wear* 304(1–2):43–48. <https://doi.org/10.1016/j.wear.2013.04.022>
17. Alemani M, Gialanella S, Straffellini G et al (2017) Dry sliding of a low steel friction material against cast iron at different loads: characterization of the friction layer and wear debris. *Wear* 376:1450–1459. <https://doi.org/10.1016/j.wear.2017.01.040>
18. Li X, Gao Y, Wei S, Yang Q (2017) Tribological behaviors of B4C-hBN ceramic composites used as pins or discs coupled with B4C ceramic under dry sliding condition. *Ceram Int* 43(1):1578–1583. <https://doi.org/10.1016/j.ceramint.2016.10.136>
19. Kennedy FE, Lu Y, Baker I (2015) Contact temperatures and their influence on wear during pin-on-disk tribotesting. *Tribol Int* 82:534–542. <https://doi.org/10.1016/j.triboint.2013.10.022>
20. Khadem M, Penkov OV, Yang HK et al (2017) Tribology of multi-layer coatings for wear reduction: a review. *Friction* 5(3):248–262. <https://doi.org/10.1007/s40544-017-0181-7>
21. Hutchings I, Shipway P (2017) *Tribology: friction and wear of engineering materials*. Elsevier, London
22. Ajayi OO, Lorenzo-Martin C, Erck RA et al (2011) Scuffing mechanism of near-surface material during lubricated severe sliding contact. *Wear* 271(9–10):1750–1753. <https://doi.org/10.1016/j.wear.2010.12.086>
23. Jha P, Gautam RK, Tyagi R (2017) Friction and wear behavior of Cu–4 wt.% Ni–TiC composites under dry sliding conditions. *Friction* 5(4):437–446. <https://doi.org/10.1007/s40544-017-0157-7>
24. Archard J (1953) Contact and rubbing of flat surfaces. *J Appl Phys* 24(8):981–988. <https://doi.org/10.1063/1.1721448>
25. Reid JV, Schey JA (1987) The effect of surface hardness on friction. *Wear* 118(1):113–125. [https://doi.org/10.1016/0043-1648\(87\)90008-1](https://doi.org/10.1016/0043-1648(87)90008-1)
26. Sullivan JL, Wong LF (1985) Wear of aluminium bronze on steel under conditions of boundary lubrication. *Tribol Int* 18(5):275–281. [https://doi.org/10.1016/0301-679X\(85\)90106-9](https://doi.org/10.1016/0301-679X(85)90106-9)

Publisher's Note Springer Nature remains neutral with regard to jurisdictional claims in published maps and institutional affiliations.